Rendering Morpho *butterflies based on high accuracy nano-optical simulation*

Naoki Okada, Dong Zhu, Dongsheng Cai, James B. Cole, Makoto Kambe & Shuichi Kinoshita

Journal of Optics

ISSN 0972-8821
Volume 42
Number 1

J Opt (2013) 42:25-36
DOI 10.1007/s12596-012-0092-y

Springer

J Opt (January–March 2013) 42(1):25–36
DOI 10.1007/s12596-012-0092-y

RESEARCH ARTICLE

Rendering *Morpho* butterflies based on high accuracy nano-optical simulation

Naoki Okada · Dong Zhu · Dongsheng Cai · James B. Cole · Makoto Kambe · Shuichi Kinoshita

Received: 3 February 2012 / Accepted: 4 October 2012 / Published online: 9 November 2012

Abstract A rendering method, based on high accuracy nano-optical simulations, is developed and applied to render the iridescent colors of the *Morpho* butterfly. The wings of the male display blue structural colors and backscatterings. In order to capture the *Morpho* butterfly features, subwavelength interactions on the scales must be rigorously taken into account. We calculate optical interference in the subwavelength scale structure using the high accuracy nonstandard finite-difference time-domain method, and validate the results by comparing with experimental measurements. Using our simulation results, realistic *Morpho* butterfly images are rendered.

Keywords *Morpho* butterfly · Iridescence · Photorealistic rendering · FDTD simulation · Physically based model

Electronic supplementary material The online version of this article (doi:10.1007/s12596-012-0092-y) contains supplementary material, which is available to authorized users.

N. Okada (✉) · D. Cai · J. B. Cole
Graduate School of Systems and Information Engineering, University of Tsukuba,
Tsukuba, Japan
e-mail: okada@cavelab.cs.tsukuba.ac.jp

D. Zhu · M. Kambe · S. Kinoshita
Graduate School of Frontier Biosciences, Osaka University, Osaka, Japan

Introduction

Color that is not produced by pigment is called structural color. An object is iridescent if its color changes with viewing angle. Structural color and iridescence are ubiquitous. Soap bubbles, compact disks, hair, skin, iris, jewel beetles, pigeons, peacocks, and butterflies all display structural color and iridescence [1–10]. These phenomena arise from the interaction of light with subwavelength features.

We focus on a male of a species of *Morpho rhetenor* butterfly, native to Central and South America, which displays a particularly brilliant iridescent blue as shown in Fig. 1. This *Morpho* blue arises from optical interference in subwavelength structures of nanometer size on the butterfly's scales. A remarkable characteristic of this structure is that it contains three photonic crystal-like structures as explained in Section 3. Phase-shift generated by three different co-existing structures gives rise to the butterfly's iridescence and backscattering (light is not specularly reflected but instead scatters back to the source).

Structural colors cannot be captured using geometrical optics, because it does not take subwavelength interference effects into account. The conventional finite-difference time-domain (FDTD) method can compute subwavelength interactions, but the computational cost is too high to accurately analyze complicated structures. We therefore used the nonstandard (NS) FDTD method [11, 12], which has much higher accuracy at lower cost for monochromatic waves.

Fig. 1 Photograph of a male *Morpho rhetenor*. Its wings have a brilliant blue color but contain no pigments

Figure 2 illustrates the pipeline used to render the *Morpho* butterfly iridescence. It can be summarized in the following steps: (1) Model the subwavelength structures based on a transmission electron microscope image; (2) Simulate light scattering from the butterfly model using the NS-FDTD method; (3) Using the near-to-far field transformation and the color system transformation, obtain the bidirectional reflectance distribution function (BRDF); (4) Render the butterfly image using the BRDF. To the best of our knowledge, this is the first time that *Morpho* butterflies have been photo-realistically rendered using a rigorous FDTD calculation validated by experimental measurements.

Previous works

The scale structure of the male *Morpho* butterfly has been studied intensively, and several groups have attempted to render its structural color [13–17]. But they fail to reproduce both the iridescent blue and its strong backscattering, because the diffraction superposition model [18] that they used cannot capture the interference effects due to the subwavelength features of the butterfly's scales.

Although subwavelength effects have not been completely ignored in conventional computer graphics (CGs), they approximate the structures by such simple regular shapes as spheres, thin films, multilayer films, and regular diffraction gratings, which can be theoretically analyzed. For example, the atmosphere [19], clouds [20], soap bubbles [21], iridescent colors in simple structures [22], and compact discs [23] have been rendered. Other examples are given in [24–27]. Since the subwavelength structures of the *Morpho* butterfly are much more complicated [13–17], its blue color cannot be reproduced using such simple structure models.

Not only are the subwavelength phenomena of *Morpho* butterflies difficult to understand theoretically, but their fabrication and measurement is also difficult [28–31]. There have been previous attempts to compute the subwavelength interactions of the *Morpho* butterfly using conventional FDTD or NS-FDTD simulations [32–34], but the computed reflectance spectra differ from experiment [31] because they used oversimplified structural models, and the rendered images failed to capture the blue iridescence and the backscattering. Using an improved structure model we were able

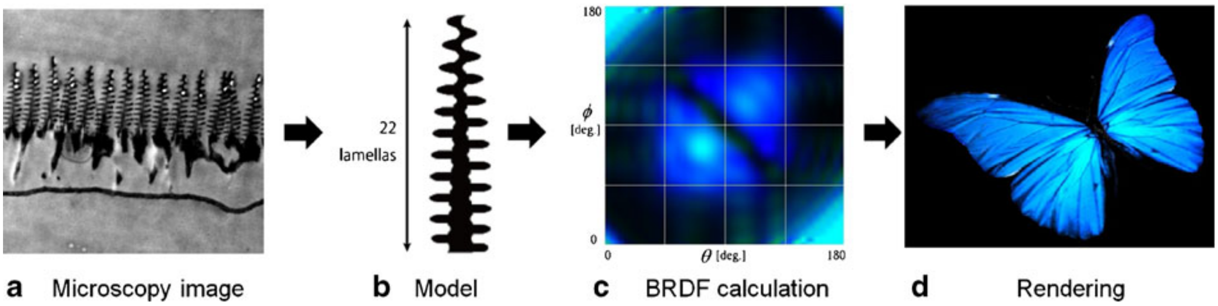

Fig. 2 Pipeline to render the structural color of a male Morpho butterfly: **a** Transmission electron microscope image of a butterfly scale. Numerous photonic crystal-like ridges are visible. **b** Model of a single ridge. Diffraction spots due to a periodic structure can be canceled out by the averaging effect of ridges with random heights on the butterfly scales. **c** Simulated nano-optics based on bidirectional reflectance distribution function (BRDF) (θ = incidence angle, ϕ = reflection angle). The BRDF is obtained using the near-to-far field transformation and the color system transformation. **d** Rendered image of a male Morpho butterfly

to improve on their results and reproduce more realistic iridescence and backscattering than previously.

Nano-structure of *Morpho* butterfly scales

The subwavelength structures of the male *Morpho rhetenor* butterfly scales is shown in Fig. 3: images (a) and (b) were made using an optical microscope and (c) is a transmission electron micrograph. Figure 3(a) shows the arrangement of scales on a wing; (b) shows a single scale; (c) shows ridges and lamellae alignments on a cross-section of the scale. The width and thickness of a lamella are about 300 nm and 100 nm in subwavelength regime, respectively. Figure 3(d) is a simplified perspective view of a scale, where lamellae are inclined at about 10° to the x-z plane. The ridges are composed of staggered lamellae like a book shelf.

Three photonic crystal-like structures coexist in the array of ridges and lamellae. The first one is a 1-D multilayer which gives rise to the blue color.

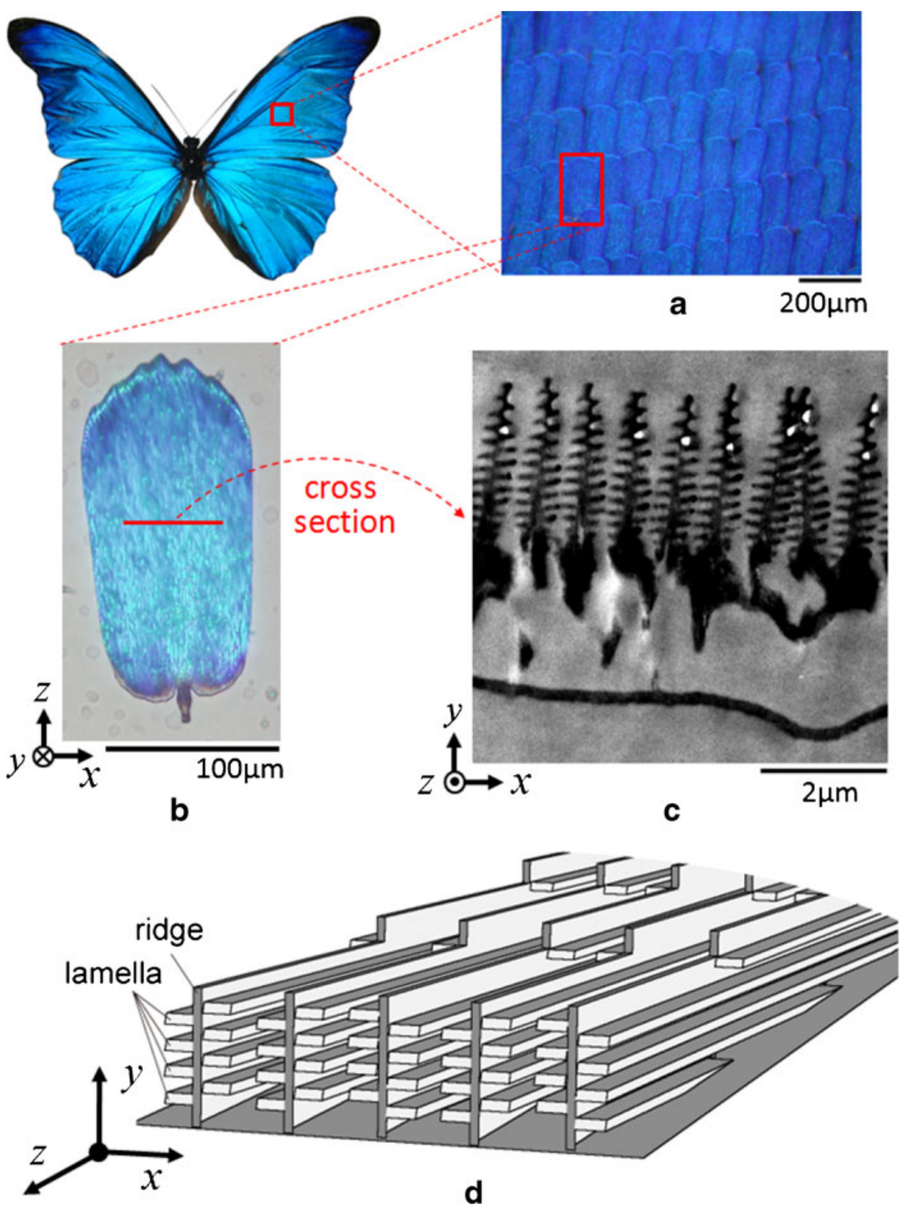

Fig. 3 Male *Morpho rhetenor* wing scales. **a** Arrangement of scales on the wing. **b** A single scale. **c** Ridges and lamellae alignments on the cross-section of a scale. **d** Simplified 3D depiction of scale structure

Thin films with air and lamellae can be approximated by a multilayer film structure. The reflected wavelength of a multilayer must satisfy [35–37]

$$n_l d_l \cos\theta_l + n_a d_a \cos\theta_a = m\lambda/2, \tag{1}$$

where n is the refractive index, d is the thickness of a film, θ is the refraction angle, λ is the incident wavelength, and m is an integer. The subscripts l and a denote the lamella and air, respectively. Given typical parameters in the microscope image, n_l=1.55, n_a=1, d_l=80 nm and d_a=115 nm in Eq. (1) and putting m=1, we obtain $\lambda\cong$480 nm (blue light) at normal incidence ($\theta_l=\theta_a=0$). The second photonic crystal-like structure causes blue light backscattering by the bookshelf-like staggered lamella on each ridge. A ridge is composed of a set of staggered lamella in the right and left sides. The staggered lamellae on a ridge form two phase-shifted photonic crystals on the left and right. These two photonic crystals interact with light in such a way that the blue component scatters back to its source [31, 33]. The third photonic crystal-like structure is a diffraction grating formed by ridges of random height. A pair of ridges can be approximated by a single slit structure. Single slit diffraction is given by

$$d_r \sin\phi = m\lambda, \tag{2}$$

where d_r is the ridge interval and ϕ is the reflection angle. Taking λ=480 nm, d_r=550 nm and m=1, we obtain a diffraction peak at $\phi\cong60°$. Although the structure of the *Morpho* butterfly is periodic, its width, height, and ridge (lamella) shape contain some randomness, which randomly shifts the phases of reflected waves and cancels out the grating effect [33].

It has been hypothesized that the coexistence of these three photonic crystal-like structures is the origin of the brilliant iridescence of the *Morpho* butterfly. But the combination of these effects is difficult to theoretically analyze and is best investigated by numerical simulations. Note that the anisotropic reflections are mainly in the x-y plane and observed by rotating the body around the z-axis as shown in Fig. 3(d). This is because many ridges uniformly extend along the z-axis.

Nonstandard FDTD algorithm

Scattering of simple structures such as spheres and infinite cylinders can be computed exactly using Mie theory [38], but scattering from such complicated structures as *Morpho* butterfly scales can only be computed numerically. This is a difficult calculation because a huge number of grid points is needed to ensure sufficient accuracy. The recent development of the nonstandard finite-difference time-domain (NS-FDTD) method now makes it possible to obtain sufficiently high accuracy at moderate computational cost [11, 12].

For reference, we now introduce a key concept of the NS-FDTD method. A one-dimensional monochromatic wave is given by

$$\psi(x,t) = e^{i(kx\pm\omega t)}, \tag{3}$$

where k is the wavenumber, and ω is the angular frequency. The conventional or standard (S) central finite difference (FD) approximation of the first derivative is given by

$$\partial_x\psi(x,t) \cong \frac{d_x\psi(x,t)}{h}, \tag{4}$$

where $\partial_x = \partial/\partial x$, h is the grid spacing, and $d_x\psi(x,t) = \psi(x+h/2,t) - \psi(x-h/2,t)$. For an arbitrary superposition of monochromatic waves, an exact central FD expression is given by

$$\partial_x\psi(x,t) = \frac{d_x\psi(x,t)}{s(k,h)}, \quad s(k,h) = \frac{2}{k}\sin\left(\frac{kh}{2}\right). \tag{5}$$

Equation (5) is called a nonstandard (NS) FD expression [39]. The NS-FD expression is equivalent to the usual definition of a derivative because,

$$\lim_{h\to0}\frac{d_x\psi(x,t)}{s(k,h)} = \lim_{h\to0}\frac{d_x\psi(x,t)}{h} = \partial_x\psi(x,t). \tag{6}$$

Similarly, there is an exact NS-FD expression for the time derivative of the form,

$$\partial_t\psi(x,t) = \frac{d_t\psi(x,t)}{s(\omega,\Delta t)}, \quad s(\omega,\Delta t) = \frac{2}{\omega}\sin\left(\frac{\omega\Delta t}{2}\right), \tag{7}$$

where Δt is the time step.

The NS-FDTD method can be extended to two and three dimensions. Although it is no longer exact, its accuracy is much higher than S-FDTD

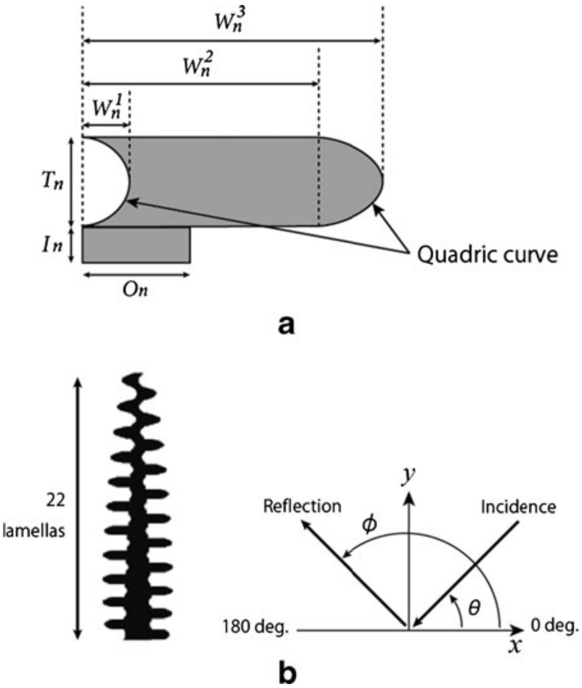

Fig. 4 A single averaged ridge that represents an entire scale in the numerical simulation. **a** Model of a single lamella on a ridge. T_n is thickness, I_n is pedestal. W_n^1, W_n^2, W_n^3 are, respectively, the widths indicated in the figure. Region O_n connects one lamella to another. **b** Single averaged ridge model (left) consisting of 22 lamellae. The incidence angle θ and reflection angle ϕ in *x-y* plane (right)

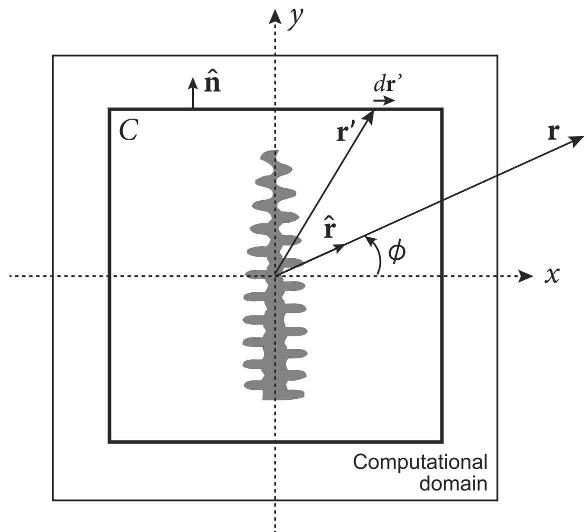

Fig. 5 Setup to calculate the near-to-far field transformation. **r** is a position vector in far field, $\widehat{r} = \mathbf{r}/|\mathbf{r}|$, ϕ is the reflection angle, C is a closed integration path, r′ is a position vector on C, $\widehat{\mathbf{n}}$ is a unit vector normal to C, and d**r′** is the perturbation on C

with respect to monochromatic waves [11]. Applying the NS-FDTD method to Maxwell's equations, we calculate light reflection from the *Morpho* butterfly's subwavelength structures.

Rendering pipeline

Nano-structure modeling

To compute its optical characteristics, we need a model of the *Morpho* butterfly scales. As discussed in Section 3, diffraction spots generated by slit interference are washed out by many ridges of random height. If only a few scales are used in the simulation, spurious diffraction spots (which the real butterfly does not display) are not washed out, but the greater the number of scales in the simulation the higher the computational cost. Fortunately, many ridges of random height are optically equivalent to one single averaged ridge [33], and thus using one averaged ridge we can model the *Morpho* butterfly scales.

Table 1 Simulation parameters

Angular range	0~180° (5° increments)
Wavelength range	350~550 nm (10 nm increments)
Grid spacing	10 nm
Computational domain	4 μm×4 μm
Refractive index	1.55

Since many ridges uniformly extend along the *z*-axis as shown in Fig. 3(d), the anisotropic reflection can be simply modeled on a two-dimensional *x-y* plane perpendicular to the wing surface. A lamella is modeled as shown in Fig. 4(a), where both ends of the lamella are approximated by a quadric curve. Averaging over a number of ridges measured in transmission electron microscope image in Fig. 3(c) and using polynomial approximations, we obtain

$$\begin{bmatrix} T_n \\ I_n \\ O_n \\ W_n^1 \\ W_n^2 \\ W_n^3 \end{bmatrix} = A \begin{bmatrix} n^4 \\ n^3 \\ n^2 \\ n \\ 1 \end{bmatrix} [nm], \tag{8}$$

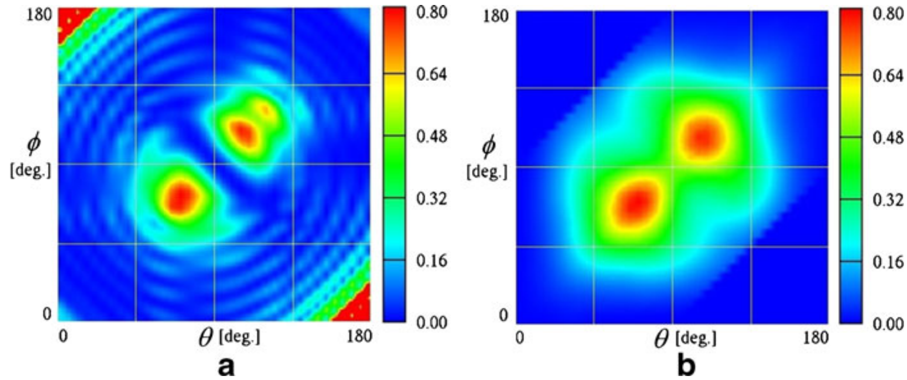

Fig. 6 The reflectance distribution at wavelength=480 nm (θ = incidence angle, ϕ = reflection angle). **a** Reflectance distribution computed by NS-FDTD simulations using a single averaged ridge. **b** Experimentally measured reflectance distribution of a 5× 5 mm^2 *Morpho* wing sample [31]. Color bars indicate the reflectance ratio

where n=1, 2,⋯, 22 is the lamella number is counted upward from the root, and

$$A = \begin{bmatrix} -0.002 & 0.09 & -0.99 & 2.73 & 75.17 \\ 0.001 & -0.05 & 0.27 & 3.33 & 2.45 \\ -0.005 & 0.24 & -3.63 & 11.18 & 211.95 \\ -0.004 & 0.17 & -2.16 & 9.72 & 11.11 \\ 0.004 & -0.16 & 0.97 & -2.82 & 316.38 \\ -0.005 & 0.22 & -3.81 & 17.80 & 359.09 \end{bmatrix} \tag{9}$$

Using the above, we obtain the averaged ridge shown in Fig. 4(b). In the figure (right), the incidence angle θ and reflection angle ϕ are defined in the two-dimensional surface with respect to this single ridge (left).

Nano-optics based BRDF calculation

Using the NS-FDTD method, we first solve the full form of Maxwell's equations to simulate the near field reflections of a single averaged ridge in both the transverse electric (TE) and transverse magnetic (TM) modes. The simulation parameters are listed in Table 1. The computational domain is terminated by the nonstandard perfectly matched layer absorbing boundary condition (8-layers) [40]. Since the BRDF or the reflectance is measured in far field, we use the near-to-far field transformation [41] to obtain the reflectance in far field. The far fields are given by (see Fig. 5)

$$E_\phi = -ZN_\phi - L_z, \quad in \quad TE\ mode \tag{10}$$

$$E_z = -ZN_z + L_\phi, \quad in \quad TM\ mode \tag{11}$$

where $Z = \sqrt{\mu/\varepsilon}$ (μ = permeability, ε = permittivity) and ϕ is the angular cylindrical coordinate. In Cartesian coordinates, N and L are defined by

$$\mathbf{N} = \sqrt{\frac{\mathrm{ik}}{8\pi|\mathbf{r}|}}\mathrm{e}^{\mathrm{ik}|\mathbf{r}|}\int_C (\widehat{\mathbf{n}} \times \mathbf{H})\mathrm{e}^{\mathrm{ik}\,\widehat{\mathbf{r}}\cdot\mathbf{r}'}\mathrm{d}\mathbf{r}', \tag{12}$$

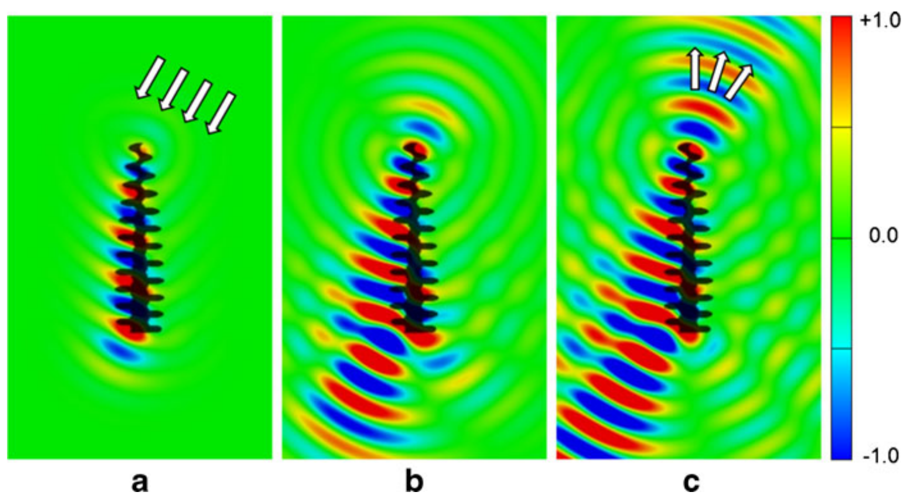

Fig. 7 Backscattering in simulation of the TM mode (wavelength=480 nm). Black region is a single averaged ridge model. **a** Parallel beam is incident at θ= 75°, indicated by white arrows, at time=3 wave periods. **b** Scattered waves interact with each other as they propagate along several direction at time=6 wave periods. **c** Interference causes backscattering indicated by white arrows at time=15 wave periods

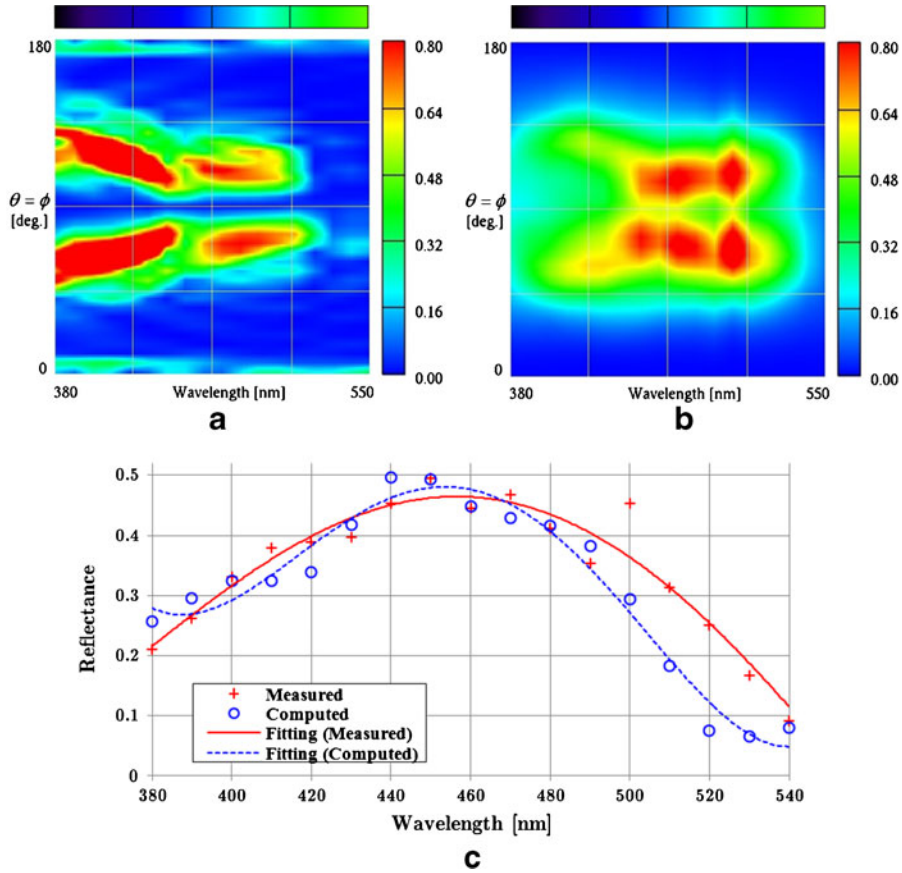

Fig. 8 The reflectance spectra of a *Morpho* butterfly scale. **a** Computed and (**b**) experimentally measured [31] spectrum distributions at $\theta=\phi$ (upper color bars denote incident light color, right bars show the reflectance ratio). **c** Angular-integrated reflectance spectrum with fitting curves at $\theta=90°$

$$\mathbf{L} = \sqrt{\frac{\mathrm{ik}}{8\pi|\mathbf{r}|}}\mathrm{e}^{\mathrm{ik}|\mathbf{r}|}\int_C (\mathbf{E}\times\widehat{\mathbf{n}})\mathrm{e}^{\mathrm{ik}\widehat{\mathbf{r}}\cdot\mathbf{r}}\mathrm{d}\mathbf{r}', \tag{13}$$

where $\mathbf{r}$ is a position vector in far field, $\widehat{\mathbf{r}} = \mathbf{r}/|\mathbf{r}|$, C is a closed integration path, $\mathbf{r}'$ is a position vector on C, and $\widehat{\mathbf{n}}$ is a unit vector normal to C. The transformation of $\mathbf{N}$ and $\mathbf{L}$ from Cartesian to cylindrical coordinates is given by

$$N_\phi = -N_x \sin\phi + N_y \cos\phi, \tag{14}$$

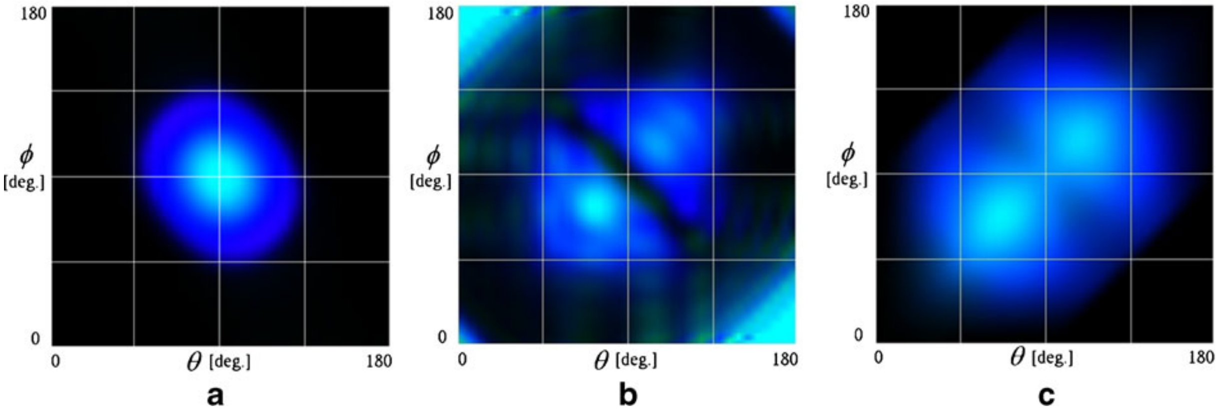

Fig. 9 BRDF color distributions in the sRGB color system: (**a**) diffraction superposition model for a single ridge (multilayer width=300 nm, interval=235 nm, and number=10) [18]; (**b**) our calculation; and (**c**) experimental measurement (θ = incidence angle, ϕ = reflection angle)

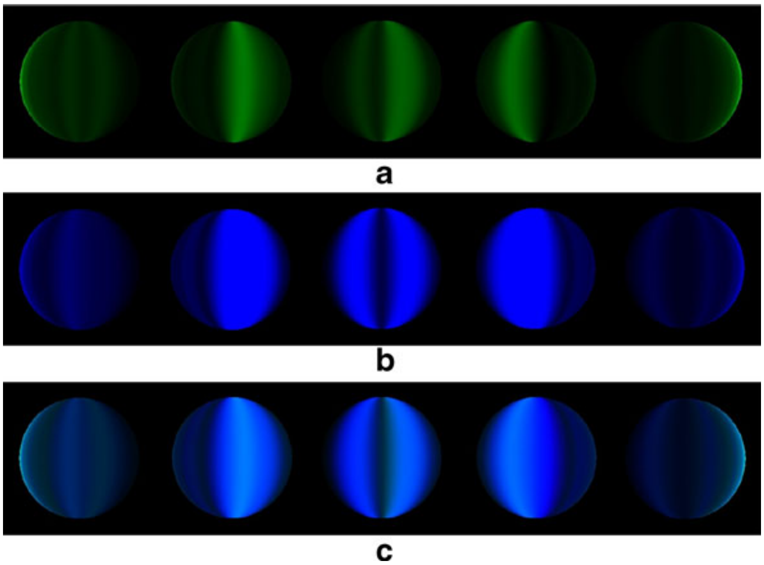

Fig. 10 Rendered color sphere using the simulated BRDF: (**a**) green; (**b**) blue; and (**c**) sRGB. From left to right, the incidence angles are, θ=30, 60, 90, 120, and 150°, respectively. The observing angle is ϕ=90°

$$L_\phi = -L_x \sin\phi + L_y \cos\phi. \tag{15}$$

The reflectance R for each angle ϕ is given by

$$R(\phi) = |E_\phi|^2 + |E_z|^2. \tag{16}$$

For all visible wavelengths λ and over all incidence angles θ, we obtain the anisotropic reflectance distribution, $R(\lambda, \theta, \phi)$. These calculations took about 10 hours on an Intel Core 2 Duo 2.66 GHz parallel CPU.

Figure 6(a) shows the reflectance distribution R computed using the NS-FDTD simulation for blue light (wavelength=480 nm). Figure 6(b) shows the experimentally measured R using a male *Morpho rhetenor* wing sample. In the experiment, the wing sample was

Fig. 11 A male *Morpho rhetenor* CG using: (**a**) Experimentally measured BRDF on flat surfaces; (**b**) Simulated BRDF on flat surfaces; (**c**) Simulated BRDF on texture- and displacement-mapped surfaces; and (**d**) Simulated BRDF combined with *Morpho* wing image. Here the incidence angle is θ=75°. From up to down, the observing angles are ϕ=150, 120, and 90°, respectively

Fig. 12 **a** Texture of the wing nervule pattern used in the texture- and displacement-mapping. **b** Photograph of the real male *Morpho* butterfly

5×5 mm^2 and the all-angle reflection method was used [31]. Both the simulated and measured results succeed in capturing the backscattering which cannot be obtained by the diffraction superposition model [18]. In the experimental measurements, there is no transmitted light because the many taper-shaped ridges channel light into the back of the wings. This has only a small effect on the rendered images due to Lambert shading as discussed in Section 5.3. Figure 7 shows an example calculation of the scattered electric field distribution with blue light backscattering (wavelength=480 nm) in the TM mode. In Fig. 7(a), a parallel beam impinges on a single ridge model at an angle of θ=75°. Figure 7 (b) shows interference by scattered waves after 6 periods. Figure 7(c) shows strong backscattering after 15 wave periods.

We compare the calculated reflectance spectrum with the experimental measurement [31]. Figure 8(a) and (b) show reflectance spectra along the backscattering diagonal $\theta=\phi$ line. As the figure shows, the simulation results and experiments differ at short wavelengths because the shorter wavelength, the greater the destructive interference between many ridges of random height. Fortunately the reflection at short wavelengths has only a small effect on the rendering of structural color, because the spectral power of daylight is relatively small in these wavelengths. Figure 8(c) shows reflectance spectra integrated over reflection angle (ϕ=0~180°) due to normally incident light, with fits to the data. Our computed angular-integrated spectrum agrees better with the experimental measurements than conventional simulations [33, 34], especially in the strongly-reflected blue region. Thus, using these computed results, we can produce a more realistic *Morpho* butterfly CG.

As discussed in Section 5.1, many ridges on a scale can be approximated by a single averaged ridge model. We assume that all scales are regularly aligned and have the homogeneous reflection properties. Therefore, the results for a single ridge model are extended to those for entire scales. Using the Commission International de L'Eclairage (CIE) of 1931 XYZ color system transformation, we can transform the reflectance distribution R into a BRDF under a standard illuminant [42]. We then transform the BRDF from the XYZ color system into the sRGB system. Figure 9 shows the BRDFs in the sRGB color system, which are given by (a) diffraction superposition model for a

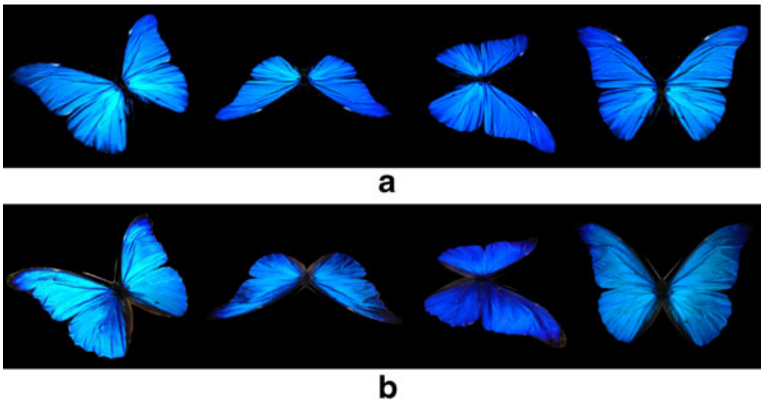

Fig. 13 Comparison of (**a**) CG images with (**b**) real photographic images from different observing angles at normal incidence (θ=90°)

Fig. 14 Rendered *Morpho rhetenor* butterfly images from different observing angles with a forest background

single ridge (multilayer width=300 nm, interval=235 nm, and number=10) [18]; (b) our calculation; and (c) experimental measurement [31]. Whereas the diffraction model fails to capture the backscattering, our result shows good agreement with the measurement. Figure 10 shows spheres rendered using the simulated BRDF. The green is reflected over a narrow angle relative to blue (red is almost zero) as shown in Fig. 10(a) and (b). In Fig. 10(c), the brilliant blue backscattering is captured.

Rendering *Morpho* butterfly images

In this section, we describe how to render male *Morpho* butterfly CGs using the simulated BRDF. Eliminating spurious transmitted light in the simulated BRDF, we use a simple Lambert shading. The reflected intensity at each surface point is given by

$$I = k_i I_i (\mathbf{N} \cdot \mathbf{L}), \quad (i = r, g, b) \tag{17}$$

where k_i is the reflectance, I_i is the incident intensity given in the scene, **N** is the unit normal vector, and **L** is the unit incidence vector. In Eq. (17), k_i is obtained from the simulated BRDF. Figure 11 displays rendered male *Morpho rhetenor* images from three different observing angles. The incidence angle is $\theta=75°$, which the brilliant *Morpho* blue is strongly reflected. Figure 11 shows rendered images using: (a) the measured BRDF on flat wing surfaces; (b) simulated BRDF on flat surfaces; (c) simulated BRDF on texture- and displacement-mapped surfaces (see Fig. 12(a)); and (d) the simulated BRDF synthesized with *Morpho* wing image. As shown in both Fig. 11(b) and (c), the rendered images capture the backscattering of the brilliant *Morpho* blue in agreement with experiment shown in Fig. 11(a). We feel, however, that the rendered CG images are monotonous because to create the CG we assumed all ridges and lamellae to be arrayed uniformly in z on the wing surface.

In order to show the complicated fuzzy iridescence of real scale distributions on *Morpho* butterfly wings, we combined the simulated BRDF with wing texture. Figure 12(b) shows the texture photographed using indirect light so that the *Morpho* blue is mainly given by the simulated BRDF. Figure 11(d) shows the final rendered CG images. In Fig. 13, we compare rendered CG images with photographs from different observing angles. Our results are an improvement over conventional methods [15], and are comparable to photographic images. Figure 14 shows photo-realistically rendered images from different observing angles with a forest background.

Finally we render the *Morpho helena*, which is the same subspecies as the *rhetenor*. The *Morpho helena* has different wing patterns from that of *rhetenor* but the scale structures are almost the same [10]. Figure 15 are rendered images of the *Morpho helena*, and are comparable to the photographic ones.

Fig. 15 Rendered images of a male *Morpho helena*

Conclusion

A pipeline to render *Morpho* butterfly iridescence, based on both rigorous modeling and nano-optical NS-FDTD simulations, have been proposed. The pipeline consists of the following 4 steps: (1) Model sub-wavelength structures from a transmission electron microscope images; (2) Simulate light scattering of the model using the NS-FDTD method; (3) Using the near-to-far field transformation and the commission international de L'Eclairage (CIE) 1931 XYZ color system transformation, obtain a nano-optics based bidirectional reflectance distribution function (BRDF); and (4) Render the *Morpho* butterfly image using the BRDF. A model of *Morpho* butterfly scales was carefully constructed at the nano-meter level. Our computed results were in better agreement with experimental measurements [31] than conventional FDTD simulations [33, 34]. CGs of the *Morphor hetenor* and *helena* were rendered photo-realistically. Furthermore, this paper has demonstrated the first FDTD simulation of the *Morpho* butterfly scales, which is comparable to experimental measurements.

Biological iridescence, structural color, and anisotropic reflection are ubiquitous in the natural world. Butterflies, peacocks, pigeons, swallow's tails, jewel beetles, and sea shells exhibit structural colors [2–4, 7, 10]. Even human hair with cuticles and iris display anisotropic colors [5, 8, 9]. These complicated iridescences are difficult to render photo-realistically, because the mechanism that produces complicated optical effects is still not well understood. Our work provides a methodology to render these effects having such iridescences.

Acknowledgments We deeply appreciate the financial support of Grant-in-Aid for Japan Society for the Promotion of Science (JSPS) Fellows.

References

1. W.K. Dai, R.C. Chang, Z.C. Shih, Fractal patern for a butterfly wing. Vis. Comput. Nat. **11**, 177–187 (1995)
2. A.R. Parker, 515 million years of structural colour. J. Optic. Pure. Appl. Optic. **2**(6), 15–28 (2000)
3. P. Vukusic, J.R. Sambles, C.R. Lawrence, R.J. Wootton, Structural colour: now you see it—now you don't. Nature **410**, 36 (2001)
4. P. Vukusic, J.R. Sambles, Photonic structures in biology. Nature **424**, 852–855 (2003)
5. A. Lefohn, R. Caruso, E. Reinhard, B. Budge, An ocularist's approach to human iris synthesis. IEEE Comput. Graph. Appl. **23**(6), 70–75 (2003)
6. J. Egholm, N. J. Christensen, A phenomenological representation of iridescent colors in butterfly wings. in *WSCG Short Communications conference proceedings* (WSCG, 2004)
7. S. Kinoshita, S. Yoshioka, *Structrual Colors in Biological Systems* (Osaka University Press, 2005)
8. M.W.Y. Lam, G.V.G. Baranoski, A predictive light transport model for the human iris. Comput. Graph. Forum **25**(3), 359–368 (2006)
9. K. Ward, F. Bertails, T. Y. Kim, S. R. Marschner, M. P. Cani, M. C. Lin, A survey on hair modeling: Styling, simulation, and rendering. IEEE Trans. Visual. Comput. Graph., **13**(2), (2007)
10. S. Kinoshita, S. Yoshioka, J. Miyazaki, Physics of structural colors. Institute of Physics (IOP) Publishing, Reports on Progress in Physics, **71**(7), 076401 (2008)
11. J.B. Cole, High-accuracy yee algorithm based on nonstandard finite differences: New developments and verifications. IEEE Trans. Antenn. Propag. **50**(9), 1185–1191 (2002)
12. N. Okada, J.B. Cole, Simulation of whispering gallery modes in the mie regime using the nonstandard finite-difference time domain algorithm. J. Optic. Soc. Am. B **27** (4), 631–639 (2010)
13. B. Gralak, G. Tayeb, S. Enoch, Morpho butterflies wings color modeled with lamellar grating theory. Opt. Express **9** (11), 567–578 (2001)
14. N. Shichijo, S. Iwasawa, Y. Kawaguchi, *Rendering methods for models with complicated micro structures. The 14th International Conference on Artificial Reality and Telexistence* (Nov. 2004)
15. Y. Sun, Rendering biological iridescences with rgb-based renderers. ACM Trans. Graph. **25**(1), 100–129 (2006)
16. I. Sadeghi, H. W. Jensen, *A physically based anisotropic iridescence model for rendering morpho butterflies photo-realistically* (UCSD Research EXPO, 2008)
17. L. Plattner, Optical properties of the scales of morpho rhetenor butterflies: theoretical and experimental investigation of the back-scattering of light in the visible spectrum. J. R. Soc. Interface **22**(1), 49–59 (2012)
18. S. Kinoshita, S. Yoshioka, Y. Fujii, N. Okamoto, Photophysics of structural color in the morpho butterflies. Forma **17**, 103–121 (2002)
19. D. Jackel, B. Walter, Modeling and rendering of the atmosphere using mie-scattering. Comput. Graph. Form **16**(4), 201–210 (1997)
20. M.J. Harris, A. Lastra, Real-time cloud rendering. EUROGRAPHICS **20**(3), 201–210 (2001)
21. K. Iwasaki, K. Matsuzawa, T. Nishita, Real-time rendering of soap bubbles taking into account light interference. in *Proceedings of the Computer Graphics International* (IEEE Computer Society, 2004), pp. 344–348
22. R. Shimada, Y. Kawaguchi, Brdf estimation system for structural colors. in *Proceedings of the 2005 international conference on Augmented tele-existence* (ACM, 2005), pp. 16–21
23. J. Egholm, N. J. Christensen, Rendering compact discs and other diffractive surfaces illuminated by linear light sources. in *Proceedings of the 4th international conference on Computer graphics and interactive techniques in Australasia and Southeast Asia* (ACM, 2006) pp. 329–332

24. J. Stam, Diffraction shaders. in *SIGGRAPH 99 Conference Proceedings, Annual Conference Series* (ACM, 1999), pp. 101–110
25. H. Hirayama, K. Kaneda, H. Yamashita, Y. Monden, An accurate illumination model for objects coated with multilayer films. in *Proceedings of Eurographics 2000 Short Presentations* (Eurographics, 2000), pp. 143–150
26. C. Lindsay, E. AGU, Physically-based real-time diffraction using spherical harmonics. in *Advances in Visual Computing*, vol 4292 (Springer, Berlin, 2006), pp. 505–517
27. S.B. Oh, S. Kashyap, R. Garg, S. Chandran, R. Raskar, Rendering wave effects with augmented light field. Comput. Graph. Forum **29**(2), 507–516 (2010)
28. A. Saito, Y. Miyamura, M. Nakajimaad Y. Ishikawa, K. Sogo, Y. Kuwahara, Y. Hirai, Reproduction of the morpho blue by nanocasting lithography. J. Vac. Sci. Tech. B, **24** (3248), (2006)
29. A. Saito, Y. Miyamura, Y. Ishikawa, J. Murase, M. A. Kasaya, Y. Kuwahara, Reproduction, mass production, and control of the morpho butterfly's blue. Proceedings SPIE, **7205**, (2009)
30. A. Saito, Material design and structural color inspired by biomimetic approach. Sci. Tech. Adv. Mat. **12**(064709), (2011)
31. M. Kambe, D. Zhu, S. Kinoshita, Origin of retroreflection from a wing of the morpho butterfly. J. Phys. Soc. Jap. **80** (5), 054801 (2011)
32. S. Banerjee, Z. Dong, Optical characterization of iridescent wings of morpho butterflies using a high accuracy nonstandard finite-difference time-domain algorithm. Optic. Rev. **14**(6), 359–361 (2007)
33. D. Zhu, S. Kinoshita, D. Cai, J.B. Cole, Investigation of structural colors in morpho butterflies using the nonstandard finite-difference time-domain method: effects of alternately stacked shelves and ridge density. Phys. Rev. **E**(80), 051924 (2009)
34. R.T. Lee, G.S. Smith, Detailed electromagnetic simulation for the structural color of butterfly wings. Appl. Opt. **48** (21), 4177–4190 (2009)
35. B. E. Smits, G. W. Meyer, Newton s colors: Simulating interference phenomena in realistic image synthesis. in *Proceedings Eurographics Workshop on Photosimulation, Realism and Physics in Computer Graphics* (Eurographics, 1990), pp. 185–194
36. J. D. Joannopoulos, R. D. Meade, J. N. Winn, *Photonic Crystals: Molding the Flow of Light* (Princeton University Press, 1995)
37. H. Tabata, K. Kumazawa, M. Funakawa, J. Takimoto, M. Akimoto, Microstructures and optical properties of scales of butterfly wings. Optic. Rev. **3**(2), 139–145 (1996)
38. P. W. Barber, S. C. Hill, *Light Scattering by Particles: Computational Methods* (World Scientific, 1989)
39. R. E. Mickens, *Nonstandard Finite Difference Models of Differential Equation* (World Scientific, 1994)
40. N. Okada, J. B. Cole, A nonstandard finite difference time domain algorithm for berenger's perfectly matched layer. Appl. Comput. Electromagnet. Soc. J. **26**(2), (2011)
41. R.J. Luebbers, D. Ryan, J. Beggs, A two-dimensional time-domain near-zone to far-zone transformation. IEEE Trans. Antenn. Propag. **40**(7), 848–851 (1992)
42. G. Wyszecki, W. S. Stiles, *Color Science: Concepts and Methods, Quantitative Data and Formulae* (Wiley-Interscience, 1982)